Photovoltaic potential assessment and ranking of rooftops segments based on LiDAR data

N. Lukač, B. Žalik and G. Štumberger

University of Maribor
Faculty of Electrical Engineering and Computer Science
Smetanova ulica 17, 2000 Maribor (Slovenia)
Fax number: +386 2220 7272, e-mail: **niko.lukac@um.si**, **borut.zalik@um.si**, **gorazd.stumberger@um.si**

Abstract This paper deals with a method for determining the rating of roofs' segments in urban areas regarding their suitability for the installation of different photovoltaic (PV) systems. In order to determine the received irradiance of individual roofs, their geometry is described based on LiDAR (Light Detection And Ranging) data, in order to estimate accurately the effect of shadowing and topography. The input irradiance is based on a Typical Meteorological Year (TMY), which is established over long-term irradiance measurements. The PV potential is then estimated by integrating estimated per-surface direct and anisotropic diffuse irradiances filtered with nonlinear efficiency characteristics of a given PV system. Afterwards, the roofs' segments are rated based on the estimated PV potential from low to high suitability. The proposed method was applied over a large urban area scanned by airborne LiDAR, and validated with local power plant, where 96.49% agreement was reached.

Key words

PV systems, PV potential, LiDAR data, TMY, Nonlinear efficiency characteristics.

1. Introduction

The purchase price of photovoltaic (PV) systems has reduced significantly in the past few years [1], while grid parity is predicted to be reached worldwide throughout the next decade [2]. Nowadays, one of the main challenges is the estimation of solar and PV potentials over multiple buildings' roofs within large-scale urban environment by considering all the influential factors of the urban context [3]. Solar potential represents the total solar irradiance that the observed surface receives in the given interval of observation (i.e. generally per-annum). Similarly, the photovoltaic (PV) potential is the amount of electric energy that the chosen PV system installed at a given surface can produce in the given interval.

Since the recent advances of remote sensing data acquisition technologies, such as LiDAR (Light Detection And Ranging), new solar and PV potential estimation methods have been developed. LiDAR is an active remote sensing technology that can be mounted on an aircraft in order to scan the topography of a wide area. A 3D georeferenced surface point can be calculated by knowing the duration between emission and re-absorption of a given laser pulse that has hit the surface. Vast point cloud surface data can be acquired, as modern LiDAR scanners can send more than 200 000 laser pulses per second. Due to the increased availability of high-resolution topographical details, many methods have been developed for estimating the solar and PV potentials by using the given data. Their main differences lie in the way topological structure data is estimated over LiDAR point cloud and other remote sensing [5]-[13]. This is especially important to extract the per-surface topographical details (i.e. slope and aspect), as well as to estimate shadowing effects from nearby obstructions. State-of-the-art methods also consider shadowing from vegetation by either using semi-transparent vegetation modelling [6] or light transmission estimation by using satellite-derived Leaf Area Index (LAI) [10]. Most of the state-of-the-art also consider only the constant efficiency of a PV module when estimating the PV potential [8]. Recently, it has been shown that it has bias in accuracy, in comparison to using the nonlinear efficiency characteristics of a PV module and a solar inverter [10].

In this paper we extend our previous work on PV potential estimation [10] over LiDAR data by proposing a novel rating of the resulting PV potential in order to measure the suitability of each roof segment. The input LiDAR data is structured into a 2.5D topological grid structure consisting of 2.5D cells in order to estimate fast shadowing and extract topographic features. The input long-term hourly measurements of global and diffuse irradiances by pyranometer are processed into a single Typical Meteorological Year (TMY). Perez anisotropic diffuse model is used to estimate the per-cell diffuse irradiance, while the direct irradiance is estimated by considering nearby shadowing effects and angle of incidence. The rooftops are segmented into areas with similar topographic properties. Then the PV potential is estimated for each rooftop segment by integrating the estimated per-cell irradiances throughout the year, while also considering instantaneous filtering with the nonlinear efficiency

characteristics of a given PV system. Finally, each rooftop is rated based on its estimated PV potential.

The paper is structured as follows. the next section describes in detail the proposed method for PV potential estimation over segmented roofs by using LiDAR data. The third section presents the results over an airborne LiDAR scan of an urban area, as well as validation of the proposed methodology. The last section concludes this paper.

2. PV Potential Estimation

At first a 2.5D grid G topological structure is established over LiDAR data with a given cell resolution res_G^2 [m²], as shown in Fig. 1. Each 2.5D cell $c_i \in G$ has a height defined as $c_i.z = \max\{p_1.z, p_2.z, ...p_m.z\}$, where p_j are LiDAR points within the given cell. Afterwards, the per-cell slope β and aspect γ angles are estimated for each cell from its normal vector, which is calculated by using the best-fit plane for all the neighbouring points [10]. In this paper, only buildings and terrain will be considered in the PV potential estimation, while vegetation and other type of obstructions will be disregarded.
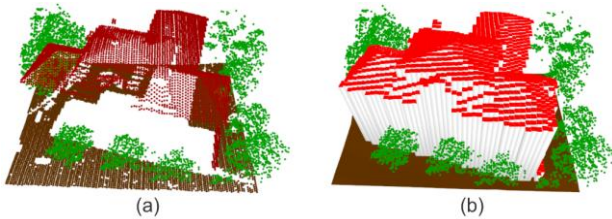

Figure 1: Example of a) classified LiDAR point cloud into buildings, terrain and vegetation, and b) the preprocessed point cloud into a 2.5D grid.

Long-term global I and diffuse I_d irradiances on a horizontal surface are obtained from the long-term measurements with an hourly time-step from a nearby meteorological station equipped with pyranometer. Based on these measurements, a TMY is estimated by using the Sandia method [15].
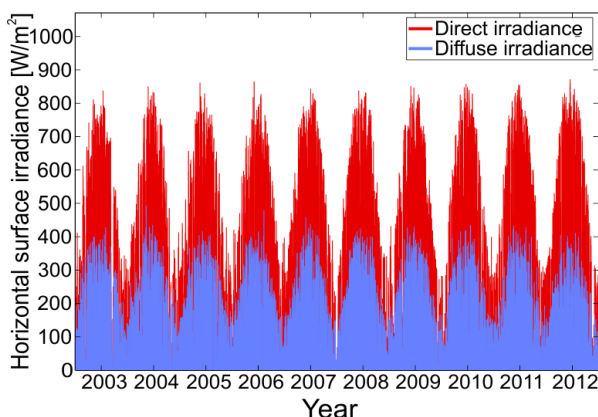

Figure 2: Yearly meteorological measurements of direct and diffuse irradiances for the time-line 2003-2012 [10].

In the continuation the TMY data is denoted with $\hat{I}$ and $\hat{I}_d$. The TMY is more robust to outliers and provides a clearer climatological data in comparison to averaging or estimating the median over the long-term measurements.

The direct irradiance $\hat{I}_b$ is estimated as $\hat{I} - \hat{I}_d$, while the reflective component is not considered in this paper. Fig. 2 shows an example of input measurements taken at a nearby meteorological station at Edvard Rusjan Airport (46° 28' 41.1" N, 15° 40' 56.0" E).

During the PV potential estimation, the spherical position of the Sun is estimated by using the Solar Positioning Algorithm (SPA) [16]. This is then transformed into Cartesian coordinates, in order to enable fast shadowing over the 2.5D grid. Instantaneous shadowing S_i of a cell c_i is estimated as [10]:

$$S_i = \begin{cases} 1 & c_i.z \le c_j.z - d_2(c_i,c_j)(q_z/\sqrt{q_x^2 + q_y^2}), \\ 0 & else \end{cases} \quad (1)$$

where c_j is the cell shadowing c_i, d_2 is a 2D Euclidean distance between the given cells, while q denotes the Sun's directional vector.

The instantaneous direct and diffuse irradiances in time instance t of a given cell c_i are estimated as:

$$I_{b_i}(t) = S_i(t)\hat{I}_b(t)R_{b_i}[\text{Wm}^{-2}], \quad (2)$$
$$I_{d_i}(t) = \hat{I}_d(t)R_{d_i}[\text{Wm}^{-2}], \quad (3)$$

where R_{b_i} and R_{d_i} are the correction factors that perturb the $\hat{I}_b$ and $\hat{I}_d$ to an arbitrary oriented and sloped surface. R_{b_i} is estimated as:

$$R_{b_i} = \frac{\cos(\theta_i)}{\cos(\theta^z)}, \quad (4)$$

θ_i and θ^z are the angle of incidence and zenith angles for a given cell c_i, respectively [17]. The R_d factor for diffuse irradiance is estimated by using anisotropic Perez diffuse model [18], which considers the influence of horizon and circumsolar brightening, as well as isotropic irradiance from the rest of the sky. The PV potential is then estimated by integrating the filtered estimated irradiance for the given cell c_i:

$$PV_i = \int_{t_1}^{t_2} \eta(I_i(t))I_i \, dt \, [\text{Whm}^{-2}], \quad (5)$$

where t_1 and t_2 define a given time-span, $I_i(t) = I_{b_i}(t) + I_{d_i}(t)$, while η is the nonlinear efficiency characteristics function of a given PV system based on [10], as shown in Fig. 3 for PV systems with three different PV modules types (i.e. A-Si for amorphous silicon, P-Si for polycrystalline silicon, and M-Si for monocrystalline silicon). The nonlinear efficiency characteristics of a PV system are obtained by combining individual PV modules (see Fig. 4) and a solar micro inverter (see Fig. 5) efficiency characteristics, which are based on least-squares nonlinear regression over sampled measurements. It should be noted that Maximum Power Point Tracking (MPPT) is considered for all efficiency characteristics.
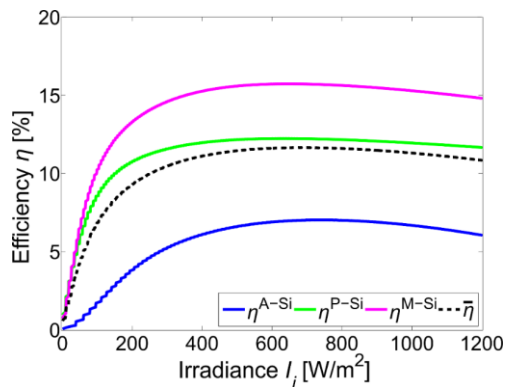
Figure 3: Nonlinear efficiency characteristics of a PV system equipped with A-Si, P-Si and M-Si types of PV modules and solar micro inverter [14].
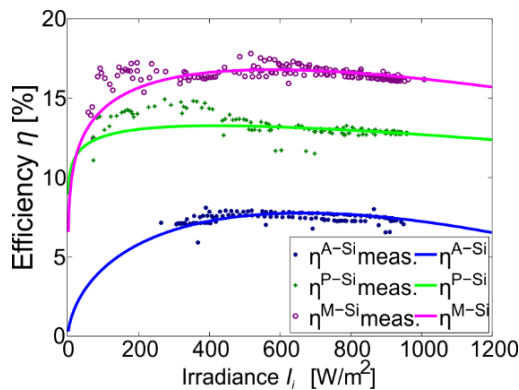

Figure 4: Nonlinear efficiency characteristics of a given PV module dependent on input global irradiance [10].
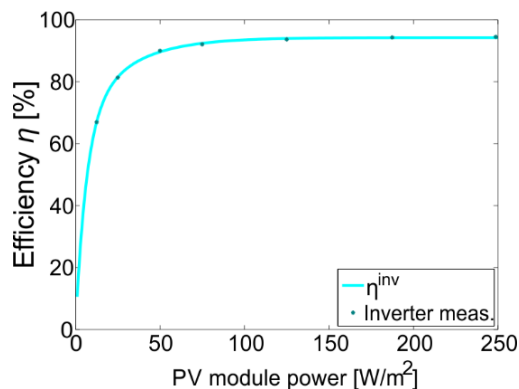

Figure 5: Nonlinear efficiency characteristics of a given solar micro inverter dependent on the electrical energy production from a given PV module [10].

Once the PV potential is estimated, the segmentation is performed over all cells that belong to the same surface on the rooftop (i.e. minimal differences in slope, orientation and height). The segmentation is performed by using the Density-Based Spatial Clustering of Applications with Noise (DBSCAN) clustering algorithm over cells' positions and normal vectors as described in [14]. The rating of each s-th segment is then defined with straightforward thresholding:

$$RT_s = \begin{cases} very\ high & PV_s/PV_{max} > 0.9 \\ high & PV_s/PV_{max} > 0.75 \\ medium & PV_s/PV_{max} > 0.5 \\ low & PV_s/PV_{max} > 0.25 \\ very\ low & PV_s/PV_{max} > 0.0 \end{cases}, \qquad (6)$$

where PV_s is the normalized sum of the PV potentials of all the cells belonging to segment s:

$$PV_s = \frac{1}{A_s}\sum_{i=1}^{n} PV_i\ [Wh], \qquad (7)$$

where A_s [m^2] is the area of the given segment. PV_{max} belongs to the segment with maximum PV potential.

3. Results

The proposed method was tested on an urban part of Maribor city, Slovenia (46° 33' 16" N, 15° 38' 48" E). Fig. 6 shows the constructed 2.5D grid model over the considered location's point cloud data obtained with airborne LiDAR. The per-cell resolution of the grid was set at $res_G^2 = 0.25$ m^2.
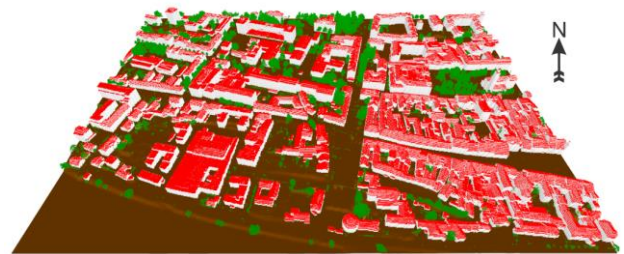

Figure 6: Visualization of the constructed 2.5D grid over the considered LiDAR scanned area.

The input long-term hourly global and diffuse irradiance measurements (See Fig. 2) were used to construct the TMY. Before the PV estimation could be performed, the buildings rooftops were segmented into areas with equal topographic properties, as shown in Fig. 7.
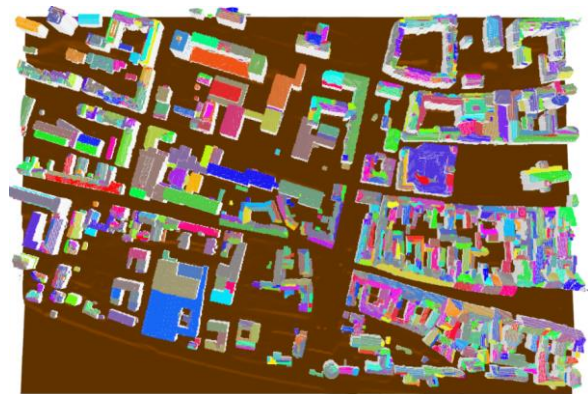

Figure 7: Segmentation of buildings rooftops in the 2.5D constructed grid. Each segment is coloured in a unique colour in comparison to its neighbouring segments.

Fig. 8 shows the results from a temporal perspective, where the daily and cumulative values for all segments in the 2.5D grid are considered. As expected hypothetical PV systems on the given segments that are using PV modules with higher efficiency yield higher production.
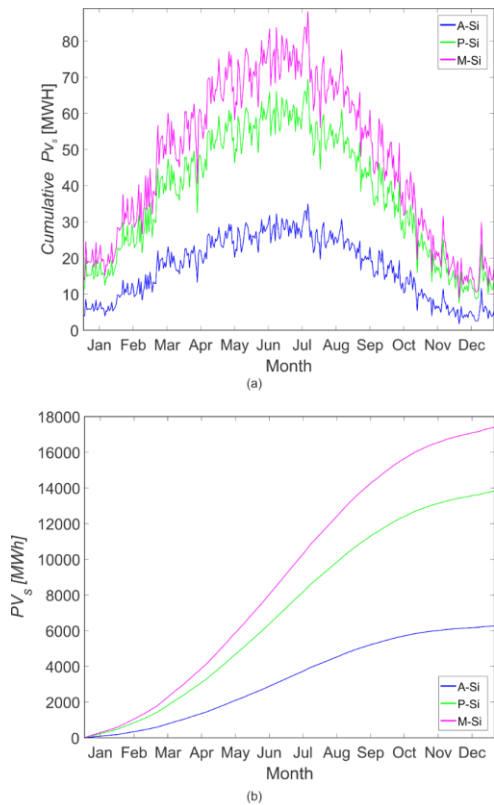
Figure 8: Estimation of a) daily PV potential and b) cumulative PV potential, of all the segments in the 2.5D grid by considering three different PV modules types.

Moreover, the proposed method was validated with average measurements of electrical energy production at a local power plant at the University of Maribor, Faculty of Electrical Engineering and Computer Science (UM-FERI), which is included in the considered LiDAR scan (see Fig 9a, b). The PV system at the power plant contains three 2.5 kWp inverters, where each is equipped with 24 M-Si 110 Wp PV modules. The results are shown in Fig. 9 c, where comparison was done with the average measured production PV_s' of segment representing the power plant, and estimated PV_s with the proposed method. The total per-annum agreement was estimated at 96.49%.
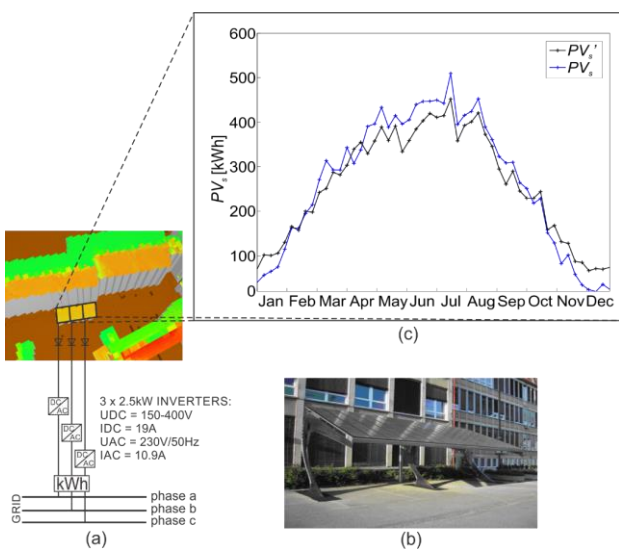

Figure 9: a, b) Local solar power plant at UM-FERI and its PV system configuration [10]; c) Comparison of estimated production with measured average per-annum production.

Finally, Fig. 10 shows the results of the ranking of the segmented rooftops based on estimated per-annum PV potential, by considering the nonlinear efficiency characteristics all three aforementioned PV modules. The PV_{max} parameter was estimated by considering the segment with maximum PV potential with an M-Si type of PV module. Hence, the results of A-Si and P-Si in Fig. 9 are relative to M-Si. As expected higher ranking is achieved by the rooftops segments that are unobstructed, oriented toward the Equator (towards the south in this case), and use M-Si type of PV module.
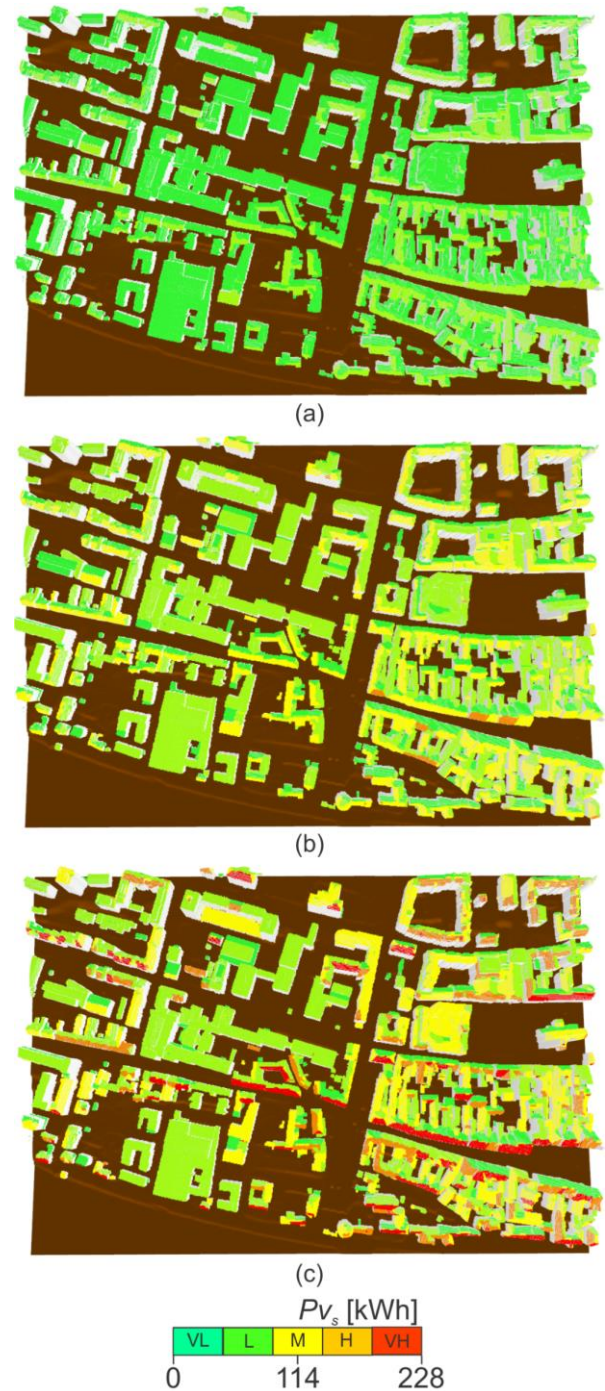

Figure 10: Rating of PV potential for segmented roofs by considering a) A-Si, b) P-Si and c) M-Si types of PV module. Legend: VL=Very Low, L=Low, M=Medium, H=High, VH=Very High.

4. Conclusion

The paper deals with the rating of roofs' segments in an urban area regarding their suitability for the installation of photovoltaic (PV) systems. The proposed method combines the classified Light Detection And Ranging (LiDAR) preprocessed data in a 2.5D grid model, Typical Meteorological Year (TMY) profile of direct and diffuse solar irradiance and nonlinear efficiency characteristics of a given PV system. The proposed rating of roofs regarding the PV potential for different PV module technologies is one of the basic steps that have to be performed in order to find optimal locations for the installation of a PV system in urban areas.

Acknowledgement

References

[1] N. S. Lewis, Toward Cost-Effective Solar Energy Use, Science 315 (5813), 2007, 798-801.

[2] M. A. Green, K. Emergy, Y. Hishikawa, W. Warta, E. D. Dunlop, Solar cell efficiency tables (version 45), Progress in photovoltaics: research and applications, 23(1), 2015, 1-9.

[3] D. Robinson, A. Stone, Solar radiation modelling in the urban context, Solar Energy, 77 (3), 2004, 295–309.

[4] G. Petrie, C. K. Toth, Topographic laser ranging and scanning: principles and processing. In: J. Shan, C. Toth, editors. Airborne and spaceborne laser profilers and scanners. CRC Press, 2008, 29-86.

[5] M. Šúri, J. Hofierka, A new GIS-based solar radiation model and its application to photovoltaic assessments, Transactions of GIS, 8 (2), 2004, 175-190.

[6] T. R. Tooke, N. C. Coops, A. Christen, O. Gurtuna, A. Preevot, Integrated irradiance modelling in the urban environment based on remotely sensed data, Solar Energy, 86 (10), 2012, 2923-2934.

[7] M. Brito, N. Gomes, T. Santos, J. Tenedorio, Photovoltaic potential in a Lisbon suburb using LiDAR data, Solar Energy, 86 (1), 2012, 283-288.

[8] H. T. Nguyen, J. M. Pearce, Incorporating shading losses in solar photovoltaic potential assessment at the municipal scale, Solar Energy, 86 (5), 2012, 1245-60.

[9] J. A. Jakubiec, C. F. Reinhart, A method for predicting city-wide electricity gains from photovoltaic panels based on LiDAR and GIS data combined with hourly Daysim simulations, Solar Energy, 93, 2013, 127-143.

[10] N. Lukač, D. Žlaus, S. Seme, G. Štumberger, B. Žalik, Buildings roofs photovoltaic potential assessment based on LiDAR (Light Detection And Ranging) data, Energy, 66, 2014, 598-609.

[11] S. Kucuksari, A. M. Khaleghi, M. Hamidi, Y. Zhang, F. Szidarovszky, G. Bayraksan, Y. Son, An integrated GIS, optimization and simulation framework for optimal PV size and location in campus area environments. Applied Energy, 113, 2014, 1601-1613.

[12] J. Gooding, R. Crook, A. S. Tomlin, Modelling of roof geometries from low-resolution LiDAR data for city-scale solar energy applications using a neighbouring buildings method, Applied Energy, 148, 2015, 93-104.

[13] S. Szabó, P. Enyedi, M. Horváth, Z. Kovács, P. Burai, T. Csoknyai, G. Szabó, Automated registration of potential locations for solar energy production with Light Detection And Ranging (LiDAR) and small format photogrammetry, Journal of Cleaner Production, 112 (part 5), 2016, 3820-3829.

[14] N. Lukač, S. Seme, K. Dežan, B. Žalik, G. Štumberger, Economic and environmental assessment of rooftops regarding suitability for photovoltaic systems installation based on remote sensing data, Energy, 107, 2016, 854-865.

[15] A. Ebrahimpour, M. Maerefat, A method for generation of typical meteorological year, Energy Conversion and Management, 51 (3), 20120, 410-417.

[16] I. Reda, A. Andreas, Solar position algorithm for solar radiation applications, Solar Energy, 76 (5), 2004, 577-89.

[17] J. A. Duffie, W. A. Beckman, Solar Engineering of Thermal Processes, Wiley-Interscience, 2006.

[18] R. Perez, R. Seals, P. Ineichen, R. Stewart, D. A. Menicucci, A new simplified version of the Perez diffuse irradiance model for tilted surfaces, Solar Energy, 39(3), 1987, 221-231.